processes

MDPI

Article

Innovative Gold/Cobalt Ferrite Nanocomposite: Physicochemical and Cytotoxicity Properties

Anna Motorzhina [1], Sonja Jovanović [2,3], Victor K. Belyaev [1,*], Dmitry Murzin [1,4], Stanislav Pshenichnikov [1], Valeria G. Kolesnikova [1,4], Alexander S. Omelyanchik [1], Lea Gazvoda [3], Matjaž Spreitzer [3], Larissa Panina [1,5], Valeria Rodionova [1,4], Marija Vukomanović [3,*] and Kateryna Levada [1]

[1] Institute of Physics Mathematics and Information Technology, Immanuel Kant Baltic Federal University, 236001 Kaliningrad, Russia; AVMotorzhina@stud.kantiana.ru (A.M.); DMurzin1@kantiana.ru (D.M.); spshenichnikov1@kantiana.ru (S.P.); vgkolesnikova1@kantiana.ru (V.G.K.); asomelyanchik@kantiana.ru (A.S.O.); drlpanina@gmail.com (L.P.); VVRodionova@kantiana.ru (V.R.); elevada@kantiana.ru (K.L.)

[2] Laboratory of Physics, Vinca Institute of Nuclear Sciences-National Institute of the Republic of Serbia, University of Belgrade, 11001 Belgrade, Serbia; sonja.jovanovic@vin.bg.ac.rs

[3] Advanced Materials Department, Jozef Stefan Institute, 1000 Ljubljana, Slovenia; lea.udovc@ijs.si (L.G.); matjaz.spreitzer@ijs.si (M.S.)

[4] The Sophia Kovalevskaya North-West Center for Mathematical Research Center, Immanuel Kant Baltic Federal University, 236016 Kaliningrad, Russia

[5] College of New Materials and Nanotechnologies, National University of Science and Technology MISiS, 119991 Moscow, Russia

* Correspondence: vbelyaev@lnmm.ru (V.K.B.); marija.vukomanovic@ijs.si (M.V.)

check for updates

Citation: Motorzhina, A.; Jovanović, S.; Belyaev, V.K.; Murzin, D.; Pshenichnikov, S.; Kolesnikova, V.G.; Omelyanchik, A.S.; Gazvoda, L.; Spreitzer, M.; Panina, L.; et al. Innovative Gold/Cobalt Ferrite Nanocomposite: Physicochemical and Cytotoxicity Properties. *Processes* **2021**, *9*, 2264. https://doi.org/10.3390/pr9122264

Academic Editors: Sergei Alexandrov, Valentina Zhukova and Arcady Zhukov

Received: 23 November 2021
Accepted: 11 December 2021
Published: 16 December 2021

Publisher's Note: MDPI stays neutral with regard to jurisdictional claims in published maps and institutional affiliations.

Abstract: The combination of plasmonic material and magnetic metal oxide nanoparticles is widely used in multifunctional nanosystems. Here we propose a method for the fabrication of a gold/cobalt ferrite nanocomposite for biomedical applications. The composite includes gold cores of ~10 nm in diameter coated with arginine, which are surrounded by small cobalt ferrite nanoparticles with diameters of ~5 nm covered with dihydrocaffeic acid. The structure and elemental composition, morphology and dimensions, magnetic and optical properties, and biocompatibility of new nanocomposite were studied. The magnetic properties of the composite are mostly determined by the superparamagnetic state of cobalt ferrite nanoparticles, and optical properties are influenced by the localized plasmon resonance in gold nanoparticles. The cytotoxicity of gold/cobalt ferrite nanocomposite was tested using T-lymphoblastic leukemia and peripheral blood mononuclear cells. Studied composite has selective citotoxic effect on cancerous cells while it has no cytotoxic effect on healtly cells. The results suggest that this material can be explored in the future for combined photothermal treatment and magnetic theranostic.

Keywords: magneto-plasmonic nanoparticles; photothermal therapy; localized plasmonic resonance

1. Introduction

Magneto-plasmonic nanoheterostructures consisting of magnetic and plasmonic materials are of great interest due to the potential applications in biomedicine, for example, in magnetic separation, magnetic resonance imaging (MRI), drug delivery, or magnetic hyperthermia combined with photothermal therapy [1,2]. Biomedical applications require particular qualities of materials such as biocompatibility, specific magnetic properties, high chemical stability, and high photothermal conversion coefficient for efficient heat generation [3,4]. The precise engineering of the nanoparticles composites' structure and materials selection should be done to achieve the desired functionality.

Among magnetic oxides, cobalt ferrites ($CoFe_2O_4$ or CFO) are remarkable magnetic materials with desirable properties for biomedicine like high magneto-crystalline anisotropy (~200 kJ/m^3), relatively high saturation magnetization (up to 90 Am^2/kg),

large Curie temperature T_C~793 K and high thermal stability [5]. It belongs to a family of $M^{2+}Fe^{3+}{}_2O_4$-type spinel ferrites (where M^{2+} is a divalent metal). The CFO nanoparticles have a moderate cytotoxicity effect on human cells if loaded into biocompatible coatings and used in proper concentrations [6–8]. Jurkat cells also show low short-term toxicity on CFO nanoparticles covered in silica [9]. It was also shown, that in low concentrations CFO nanoparticles without any covering with diameters below 10 nm show almost no inhibition of cell proliferation or general toxic effects, still accumulating in cells intracellularly and perinuclearly [10]. However, if the size of CFO nanoparticles exceeds 10 nm, they have toxic effects on cells [10,11].

The combination of magnetic and high photothermal conversion properties [12,13] can be achieved by combining gold and CFO nanoparticles in a form of core/shell [14,15] or cluster structures [16,17]. In literature, there are only two main approaches for Au and CFO nanoparticles' composite fabrication. The first is the deposition of gold species onto the CFO nanoparticles by one-pot gold reduction from chloroauric acid ($HAuCl_4$) solution, forming a core/shell structure [18]. The second is the adsorption of gold seeds/nanoparticles on the surface of CFO, forming clusters of gold nanoparticles on a surface of magnetic nanoparticles [17,19]. However, both synthesis methods are complicated and require precise control of nanoparticles' growth. One of the solutions may lay in a separate synthesis of gold and CFO nanoparticles followed with their further combination in a single composite by the means of gold and CFO nanoparticles organic coating [17,20,21].

Gold nanoparticles in Au/CFO nanocomposites have specific optical properties associated with localized plasmon resonance. Due to preferential interaction with electromagnetic fields, they found vast application in biomedical areas including imaging, sensing, drug delivery and hyperthermia treatment [22–24]. Combined with excellent biocompatibility and photostability [25,26], they have a high potential for cancer therapy [27,28]. In particular, gold nanoparticles are preferable for photothermal therapy, because of the extremely efficient conversion of light into heat under the condition of the localized plasmon resonance excitation. Gold nanoparticles absorption and light energy to heat conversion depend on the optical extinction cross-section. For gold nanoparticles, there is a size threshold at about 70–100 nm below which the absorption cross-section becomes larger. If the gold particle size is smaller than about 30 nm, they behave as pure plasmon absorbers.

In gold nanoparticles of a spherical shape, the plasmonic resonance's wavelength is about 520 nm. However, a more suitable spectral region is 700–900 nm, where body tissues are less optically dense and the light penetration depth reaches a few centimeters [29] (while deeper tissues can be reached with the use of special optical fibers [24]). The spectral position of the plasmonic resonance and light absorption in this spectral region can be tuned by changing the particle shape or surrounding medium. Due to the large fraction of surface atoms of nanoparticles over the total, the plasmonic resonance's position is very sensitive to the environmental permittivity ε_{ex} [30]. If gold nanoparticles are combined with CFO nanoparticles in a form of composite, the plasmonic resonance wavelength is shifted [31–36]. In this case, the plasmonic resonance experiences the spectral redshift caused by the change of real part of ε_{ex} and additional relaxation due to the change of imaginary part of ε_{ex}. Therefore, the presence of ferrite nanoparticles in different combinations and concentrations not only brings magnetic properties to the system but can be used to tune the optical properties of such composites.

In this article, a new approach for the preparation of gold and CFO nanocomposite is proposed. The composite consists of gold nanoparticles with diameters of 10 nm, covered with arginine and CFO nanoparticles with a diameter of 5 nm coated with dihydrocaffeic acid (DHCA). Due to the size, synthesized gold nanoparticles are expected to behave as good absorbers. The studied structural, magnetic and optical properties, as well as cytotoxicity of the prepared composites, suggest their possible biomedical applications. Particularly, the material could be explored in the future for combined photothermal therapy [37,38] and magnetic hyperthermia [39,40]. This treatment can also be combined

with the functionalization of gold nanoparticles with anticancer drugs to diagnose tumors using MRI [41–43].

2. Materials and Methods

2.1. Synthesis of Nanoparticles

For the synthesis of CFO nanoparticles, 10 mmol of the sodium hydroxide (NaOH, ApplChem, Darmstadt, Germany) were dissolved in 2 mL of distilled water and autoclaved in a 50 mL autoclave tube. Then 10 mL of 1-pentanol ($CH_3(CH_2)_4OH$, Sigma Aldrich, Saint Louis, MO, USA) were stirred in a sodium hydroxide water solution and mixed with 3.8 mL of oleic acid ($C_{18}H_{34}O_2$, Alfa Aeser, Ward Hill, MA, USA) served as a capping agent. After that, 2 mmol of iron nitrate ($Fe(NO_3)_3 \cdot 9H_2O$, Alfa Aeser, Ward Hill, MA, USA) and 1 mmol of cobalt nitrate ($Co(NO_3)_2 \cdot 6H_2O$, Alfa Aeser, Ward Hill, MA, USA) were dissolved into 18 mL of distilled water and stirred into the previously mentioned solution for 2 h. The received solution was autoclaved at 180 °C for 8 h [44]. Finally, the system was cooled to room temperature.

Cobalt ferrite nanoparticles were separated from the suspension with a permanent magnet after the residual liquid was discarded. Obtained nanoparticles were washed three times in n-hexane (C_6H_{14}, Merck, ACS, Darmstadt, Germany) with ethanol. The permanent magnet was used to separate nanoparticles from the liquid phase with each wash. Washed nanoparticles were redispersed in n-hexane and left to dry on a watch glass overnight [44].

The process of dihydrocaffeic acid coating of obtained magnetic nanoparticles is the ligand exchange reaction where dihydrocaffeic acid was replacing oleic acid. Firstly, 100 mg of dihydrocaffeic acid ($C_9H_{10}O_4$, Sigma Aldrich, MO, Saint Louis, USA) were dissolved in 10 mL of tetrahydrofuran (C_4H_8O, THF, Fisher Scientific, Pittsburgh, PA, USA). Then, the solution of nanoparticles dispersed in 4 mL of tetrahydrofuran was added dropwise into dihydrocaffeic acid solution. To complete the reaction, the resulting mixture was stirred for 3 h at 50 °C. For nanoparticle precipitation, 0.5 mL of sodium hydroxide solution (0.5 mol/L) was added to the nanoparticles mixture during the cooling process. The obtained solution was cooled up to room temperature and then centrifuged to collect nanoparticles. Coated magnetic nanoparticles were redispersed in water and stored at 4 °C. Dihydrocaffeic acid coating provides hydrophilic properties to the nanoparticles [45].

The composite of magnetic and gold nanoparticles was synthesized using the sonochemical method [46]. Firstly, 1.3 mL of dihydrocaffeic-capped, hydrophilic CFO nanoparticles were dispersed in 50 mL of water and 2 mL of 2-propanol by sonication at 25 °C for 10 min with pulsation-to-relaxation periods on:off = 2:1, 20 kHz frequency and 80% amplitude. After that 50 mL of the 0.8 mg/mL water solution of chloroauric acid ($HAuCl_4$, 50% metal basis, Sigma Aldrich, Saint Louis, MO, USA) with the same amount of arginine ($C_6H_{14}N_4O_2$, >98%, Sigma Aldrich, Saint Louis, MO, USA) were mixed with magnetic nanoparticles dispersion and sonicated for 30 min. The resulting composite nanoparticles were separated from the supernatant after centrifugation at $2.8\times g$ for 15 min and dried in air on the glass slides. The resulting composite made of CFO nanoparticles covered with dihydrocaffeic acid and gold nanoparticles covered with arginine is hereinafter referred to as Au/CFO composite.

2.2. Characterization Methods

The study of nanoparticles' morphology and size in the Au/CFO composite was carried out using transmission electron microscopy (TEM) JEM-2100 by JEOL at the accelerating voltage of 200 kV. Firstly, nanoparticle powder was dispersed in n-hexane and re-agglomerated for 10 min with ultrasonic treatment. Then the suspension of nanoparticles was put on the carbon-coated copper grid and dried in air. The size distributions were obtained using ImageJ software.

The elemental composition of the CFO nanoparticles was checked using inductively coupled plasma optical emission spectroscopy (ICP-OES) with an iCAP 6300 DUP ICP-OES spectrometer by Thermo Scientific.

The zeta-potential was measured in water suspensions of CFO nanoparticles (~0.01 mg/mL) as a function of the pH using a ZetaPALS instrument (Brookhaven Instruments Corporation). The pH of the suspension was set with HCl.

Structural characterization of CFO nanoparticles and Au/CFO composite was done by X-ray diffraction (XRD) analysis using the AXRD Benchtop Powder X-Ray Diffractometer (PROTO Manufacturing). The XRD data were recorded within the 2θ range from 30 to 90 degrees with a step of 0.015° and a 5 s/step computation time using Cu Kα radiation with a wavelength of 1.54184 Å. The XRD results were analyzed with QualX software [31].

The elemental composition of the CFO nanoparticles and Au/CFO was studied using the energy-dispersive X-Ray (EDX) spectroscopy with the EDX Bruker Quantax 75. The powder of CFO nanoparticles on the carbon tape was used. EDX studies were carried out using ESPRIT Compact software.

Magnetic properties of CFO nanoparticles and Au/CFO were studied using LakeShore 7400 vibrating sample magnetometer. Magnetization reversal of nanoparticles was measured at room temperature with the maximum applied field of 1 T. The vibrating sample magnetometer had a noise floor of 10^{-6} emu at 3 s/pt.

Optical properties of the CFO/Au were studied with the visible light absorbance spectroscopy method in the wavelength range from 370 nm to 850 nm. The experimental setup consisted of a halogen lamp with the MS5204i monochromator as a light source, an optomechanical chopper for light beam modulation with the frequency of 423 Hz, a 3500 μL square fused quartz cuvette with the 10 mm transmitted path length, and the PMM02 photomultiplier tube with SR830 Lock-in amplifier as a detecting system. For optical measurements, composites were dispersed in distilled water in three concentrations: 10 μg/mL, 50 μg/mL, and 100 μg/mL. The absorption spectra were deduced from the Beer–Lambert–Bouguer law:

$$Absorption = Log_{10}(\frac{I_0}{I})\cdot 100\%, \quad (1)$$

where I_0 is the incident light's intensity and I is the intensity of light transmitted through the cuvette with a composite solution. An absorbance spectrum of the quartz cuvette with water was subtracted from all measured spectra.

The absorption properties of the composites were numerically analyzed in the quasistatic approximation since the particle size is smaller than the skin depth. The electric field of light penetrates inside the particles and polarizes the conduction electrons. Their oscillations with respect to positively charged lattice, which occur in the particle volume, constitute the localized plasmons. Their behavior is described by the particle polarizability α induced by the electric field E_0 of light. For a particle of an ellipsoidal shape having the permittivity ε_m which is placed in a medium with the permittivity of ε_{ex} and excited by E_0, the electric field inside it is uniform and is defined as:

$$E_m = \frac{\varepsilon_{ex} E_0}{(1-N)\varepsilon_{ex} + N\varepsilon_m}, \quad (2)$$

In (2), N is the depolarization factor along E_0. For a spherical shape, $N = 1/3$. The electric polarization of the particle $P = E_m(\varepsilon_m - \varepsilon_{ex})$ defines the particle polarizability $\alpha = P/E_0$:

$$\alpha = \frac{\varepsilon_{ex}(\varepsilon_m - \varepsilon_{ex})}{(1-N)\varepsilon_{ex} + N\varepsilon_m}, \quad (3)$$

In Equations (2) and (3) the permittivity parameters are functions of the wavelength λ. The metal permittivity is a complex-valued quantity having a negative real part. At a certain wavelength, the real part of the denominator in (3) turns to zero. This corresponds to a resonance when the light is able to excite the localised plasmonic resonance. At this condition, the extinction cross-section is maximal and can be much higher than the particle cross section. It is also seen that the environment permittivity shifts the resonance to higher

wavelengths, as observed in the experiment. The absorption cross-section which defines the efficiency of photothermal conversion is defined as [47]:

$$\sigma_{abs} = 8\pi^2 Im(\alpha) V_{part}/\lambda, \quad (4)$$

where V_{part} is the particle volume.

2.3. Cytotoxicity Analysis

Cytotoxicity of synthesized nanoparticles was tested on the Human T-lymphoblastic leukemia cell line (Jurkat) and Peripheral blood mononuclear cells (PBMC). Jurkat cells were obtained from the Russian Cell Culture Collection (Institute of Cytology RAS, Saint-Petersburg, Russia). The fourth and fifth cell passages of Jurkat cell lines were used for experiments. PBMC of healthy donors (permission no. 5 from 16 May 2016; the Local Ethics Committee, Innovation park, Immanuel Kant Baltic Federal University) were isolated by density gradient centrifugation from the whole blood using Ficoll (Diacoll, Dia-M, Saint-Petersburg, Russia). Whole blood was diluted in phosphate-buffered saline (PBS) in proportion 1:3. Then diluted cell suspension was layered on ficoll (same volume as PBS) in a 50 mL conical tube. The sample was centrifuged at 400× g for 40 min without brake. Obtained PBMC were carefully transferred into a new tube and washed with PBS twice. Cells were cultured in RPMI 1640 suspension, supplemented with 10% fetal bovine serum, 0.3 mg/mL L-glutamine (all Sigma Aldrich, Saint Louis, MO, USA), and 1% penicillin and streptomycin. Cells were incubated in a 5% CO_2, and 37 °C humidified atmosphere. Before each experiment cellular survival was checked using Trypan blue staining 0.4% (Invitrogen, Waltham, MA, USA).

The cytotoxicity of nanoparticles was measured using a WST-1 (Roche Diagnostics GmbH, Germany) test after 2, 4, 8, 24, and 48 h of exposure with tested nanomaterials. The assay is based on measuring the optical density difference between light red tetrazolium salt WST-1 converted by viable cells into the yellow formazan derivative. Formazan concentration in cell suspension is in direct ratio to the viable cell concentration. Both cell lines were seeded at a density of 5×10^5 cells per ml in 96 well microplates with 100 µL of cell suspension per well. Composites suspensions with concentrations of 10, 50, and 100 µg/mL were added 10 µL per each well. The control groups were prepared in absence of nanomaterials. Each experiment was conducted six times independently. During the last 2 h of exposure, 10 µL of WST-1 reagent was added. Absorbance was measured at 450 nm in a microplate reader Bio-Rad 680. All cytotoxicity results were obtained by subtraction of blank wells absorbance from experimental wells absorbance to eliminate the influence of nanoparticles and cell medium. Blank wells consist of cell medium (for control) and cell medium suspension of nanoparticles (for experiment) were used.

2.4. Statistical Analysis

All cytotoxicity results are presented as mean with a standard deviation. A nonparametric Kruskal-Wallis test followed by a Dunn's multiple comparisons test using GraphPad Prism v.7.04 was used to compare each group to the control group.

3. Results and Discussions

3.1. Physical Properties

At the first step of the Au/CFO composite preparation, CFO nanoparticles covered with an oleic acid were synthesized. The structure and magnetic properties of these nanoparticles are discussed in the previous work [48]. These nanoparticles are very stable and non-agglomerated. They were characterized by their hydrophobicity, which is a limiting factor for their application in the formation of a composite with nanogold using water chloroauric acid. Also, this is a very limiting factor for their effective use in water-based cell environment. For that reason, a very precise ligand exchange protocol was applied for replacing oleic acid from their surface with dihydrocaffeic acid while maintaining their structural and morphological stability. At this stage, ICP-OES and EDX analysis were

used to check the CFO's composition purity. ICP-OES analysis showed Co:Fe ratio of 1.04:1.96 in the nanoparticles and the result of the EDX measurements showed the presence of cobalt, iron, oxygen, aluminum, carbon and sodium. The presence of aluminum and carbon is related to the sample holder with carbon tape on top of it. The sodium peak is due to the leftovers of the washing liquid (sodium hydroxide). EDX spectra can be found in Supplementary Materials. The last step was the reduction of gold nanoparticles on the surface of the CFO, acting as nucleation seeds, with application of arginine as gold reduction and functionalization agent. This step resulted in the formation of Au/CFO composite. The results of TEM, XRD, VSM and zeta potential (ζ) measurements for the Au/CFO are shown in Figure 1.

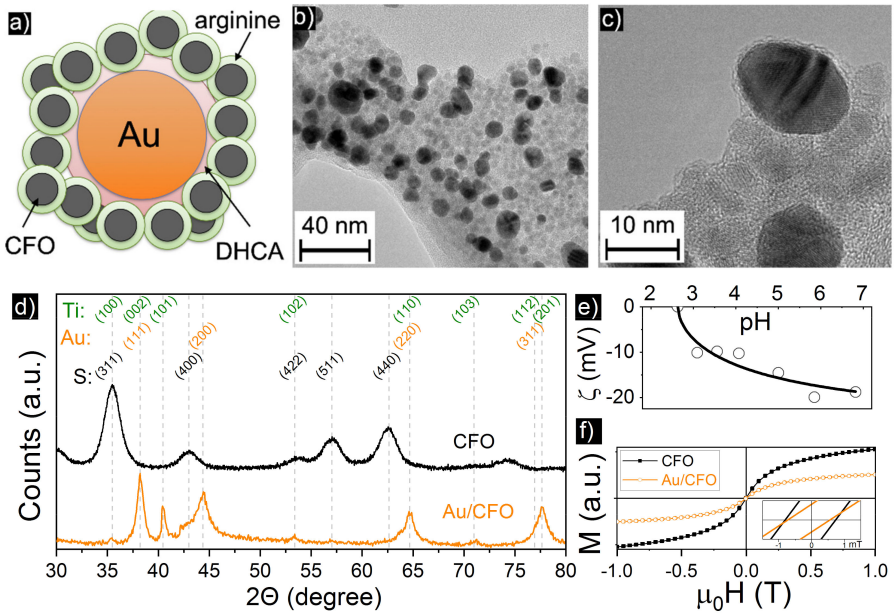

Figure 1. (**a**) Schematic representation of a gold sphere covered with arginine and surrounded with CFO nanoparticles covered with dihydrocaffeic acid; (**b**,**c**) TEM images of the Au/CFO composite; (**d**) XRD spectra for CFO nanoparticles [48] and Au/CFO composite. Reflections corresponding to titan (Ti), gold (Au) and spinel (S) phases are indexed; (**e**) zeta potential for CFO nanoparticles covered with dihydrocaffeic acid; (**f**) *M-H* loops for CFO nanoparticles and CFO\Au composite recorded at 300 K.

According to the TEM images, Au/CFO composite consisted of particles with a quasi-spherical shape. Synthesized nanoparticles were in close contact with each other due to the interaction of the dihydrocaffeic acid coating of CFO nanoparticles (light grey spheroids) with the arginine coating of gold particles (dark spheroids). Zeta potential ζ (Figure 1e) for CFO nanoparticles coated with DHCA showed negative values at different pH. In contrast, the synthesized gold nanoparticles coated with arginine had a positively charged surface [46]. The presence of both positive and negative surface charges in one solution led to the attraction between the particles.

CFO nanoparticles showed a narrow size and shape distribution with an average size of 4.9 ± 0.9 nm. Conversely, gold nanoparticles with an average size of 10.5 ± 2.6 nm showed a wider size distribution. The structural XRD study of the composite showed two phases, corresponding to gold at 2θ = 38.2°, 44.4°, 64.7°, 77.6° and titanium 2θ = 35.5°, 40.4°, 53.4°, 71.2°, 81.9° in the synthesized samples. The peaks' position was in agreement with the POW_COD database. The detected Ti-phase is a common impurity eroded by sonication Ti-tip during sonochemical synthesis. The XRD reflections of the spinel structure of CFO were hindered by titanium and gold reflections which have the similar angle position and much higher intencity. The presence of ferrimagnetic CFO phase was proved with the EDX measurements (see Supplementary Materials).

To additionally verify the presence of a magnetic phase, the *M-H* loops of the CFO nanoparticles and Au/CFO nanocomposite (Figure 1e) were measured at room temperature (~300 K). Magnetic properties of the synthesized composite depend on CFO particles' magnetic state. The measured *M-H* loop of the Au/CFO composite showed almost hysteresis-free (superparamagnetic) behavior with a small coercive force (<1 mT), that agrees with literature data for single-domain CFO nanoparticles with diameters approximately of 5 nm [48]. Such single-domain nanoparticles can produce heat if exposed to the high-frequency alternating magnetic field, depending on the material properties and surroundings of the particles [49,50].

The presence of localized plasmon resonance peak providing the possibility of photothermal conversion was experimentally and numerically analyzed in the quasistatic approximation. The experimental absorption spectra and calculated extinction cross sectionare shown in Figure 2.

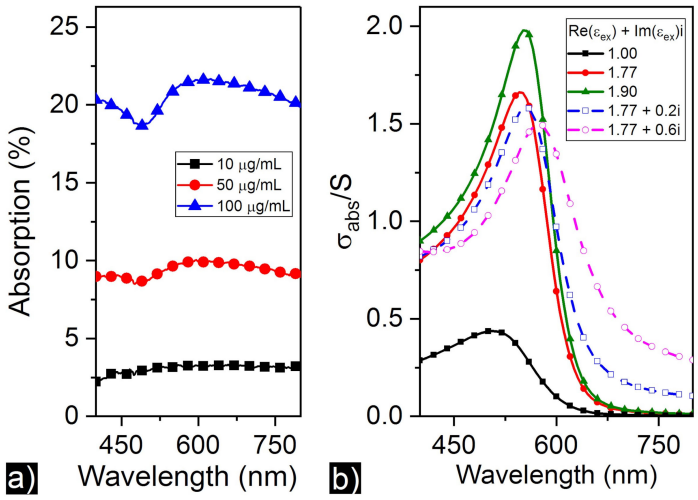

Figure 2. (**a**) Experimental absorption spectra for Au/CFO nanocomposite with different concentrations; (**b**) Calculated extinction cross section with Equation (4) for gold spherical nanparticles of 10 nm in diameter in environment with different ε_{ex}.

Experimental absorption spectra (Figure 2a) for different concentrations of the composite had a characteristic localized surface plasmon resonance peak at the wavelength of 600 nm, decreasing with the nanoparticles concentration reduction. In comparison to the characteristic absorbance spectra for gold nanoparticles with a diameter less than 10 nm, the observed plasmonic resonance was broadened and red-shifted [27,51,52]. Broadening and red-shifting of plasmonic resonance can be explained by CFO and gold nanoparticles bonding, influencing the permittivity of gold nanoparticles' surroundings [31–36]. The increase of $Re(\varepsilon_{ex})$ leads to higher values of σ_{abs}/S, where S is the cross-section of nanoparticles, and the increase of $Im(\varepsilon_{ex})$ causes broadening and damping of the plasmon resonance peak in accordance with Equations (3) and (4) (Figure 2b). This can also be considered as gold nanoparticles' conduction band electrons tunneling into the projected density of states of CFO nanoparticles [53,54]. Such interface decay channel, responsible for charge transfer to the projected density of states, modifies the relaxation time of plasmonic band's electrons and the Drude dielectric function, respectively [30].

For photothermal effects, the increase in absorption and red-shift of the localized plasmon resonance are important. The increase of absorption influences the heat release while the red-shifting can be used to move the resonance's spectral position closer to biological transparency windows. The studied magnetic and optical properties of the Au/CFO nanocomposite are well suited for combined magnetic hyperthermia and photothermal therapy. In this case, the heating effect can be enhanced up to 15 times [12,13]. To assess the compatibility/cytotoxicity of the Au/CFO nanocomposite with different

types of cells, necessary for therapeutic applications, the cytotoxicity analysis was done with Jurkat and PBMC cells that were used as models of cancer and cells in physiological condition respectively.

3.2. Cytotoxicity Analysis

Pure cobalt ferrite nanoparticles bring geno- and cytotoxic reactions in various organisms such as plants, animals, and humans [55]. Their toxic effect is shown to be independent of Co-ion release (due to very low solubility) [55] It is mainly according to the properties of the particles (including size, shape, crystal structure, surface chemistry and charge) [56]. The effect is also varying greatly depending on the cell type [55]. However, coatings can reduce cytotoxic effect for various cell cutures [57–60]. Thus, we can expect both cytotoxic or noncytotoxic effects of Au/CFO nanocomposite by using different cell cultures. In addition, gold is known as bioinert material and used in implants in various areas of medicine or as an imaging contrast [61]. Gold nanoparticles for optical hyperthermia were approved by the FDA (U.S. Food and Drug Administration) [62].

Primary observations on the cytocompatibility of foreign materials in vitro are usually carring out with leukocytes and immune-modulatory cells (e.g., PBMCs) due to the natural activity of nanoparticles uptake by these types of cells [63]. For our study, Jurkat cells (T-lymphoblastic leukemia)and PBMCs were used to determine the cytotoxic effect of Au/CFO nanocomposite. First, cobalt ferrite nanoparticles coated with dihydrocaffeic acid were tested for cytotoxicity on Jurkat cells. This was done to examine the influence of the magnetic part of nanocomposite on cells. Both CFO nanoparticles and Au/CFO nanocomposite were incubated for 2, 4, 8, 24, and 48 h with different concentrations (10, 50, 100 µg/mL). The obtained results showed that CFO nanoparticles coated with dihydrocaffeic acid were noncytotoxic for Jurkat cells after 24 h of exposure ($p \leq 0.0332$, see Supplementary Materials). In contrast, Au/CFO nanocomposite showed significant toxicity for the same exposure time ($p \leq 0.0332$).

According to the initial results (Figure 3a), Au/CFO shows a cytotoxic tendency for Jurkat cells for all exposure times except 48 h. After 48 h of incubation nanocomposite shows a noncytotoxic effect which could be explained by active cell proliferation. All further experiments were carried out for 24 h exposure time. Obtained results of Jurkat (Figure 3b) and PBMC (Figure 3c) viability are shown as a function of Au/CFO nanocomposite concentrations. Figure 3b demonstrates a dose-dependent reduction in WST-1 absorbance in Jurkat cells treated with various concentrations of nanocomposite. Treatment with 100 µg/mL Au/CFO nanocomposite showed 85% of viability, proving the cytotoxicity of this nanocomposite. In contrary, the effect on viability of PBMCs (Figure 3c) was not statistically proved and showed only insignificant fluctuations. Thus, we can assume that Au/CFO nanocomposite is more cytotoxic for Jurkat cells and has fewer effects on nonmalignant PBMCs. The nanocomposite's cyttoxicity on cancer cells could boost the effects of photothermal therapy and magnetic hyperthermia.

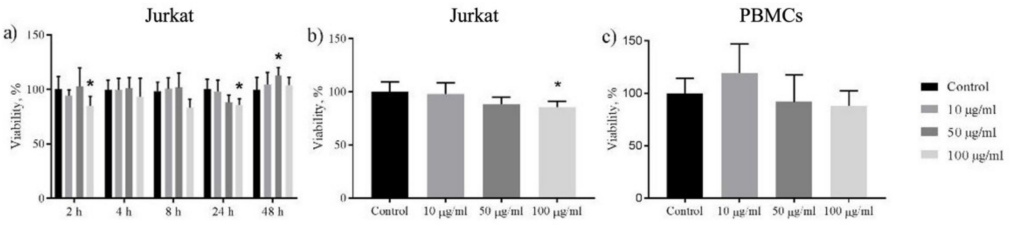

Figure 3. Viability of Jurkat cells: (**a**) after 2, 4, 8, 24 and 48 h treatment with 10, 50, and 100 µg/mL suspension of Au/CFO; (**b**) after 24 h treatment with 10, 50, and 100 µg/mL suspension of Au/CFO; (**c**) viability of PBMCs after 24 h treatment with 10, 50, and 100 µg/mL suspension of Au/CFO. Cell viability was tested by WST-1 assay. All results are normalized by control and columns denoted by asterisks indicate results that were statistically different from the control (* for p value < 0.0332). Control wells were with the absence of nanocomposites.

4. Conclusions

A new fabrication approach of Au/CFO nanocomposite was proposed based on the electrostatic assembly of positively charged arginine-coated gold cores with negatively charged cobalt ferrite nanoparticles covered with dihydrocaffeic acid. The TEM investigations showed a narrow size distribution of gold and CFO nanoparticles, which maintained the structural and morphological stability after the formation of the Au/CFO nanocomposite. The significant cytotoxicity on cancer cells and the tollerance with PBMCs cells of Au/CFO nanocomposite, combined with the magnetic properties and the presence of localized plasmon resonance peak, make it viable for several biomedical applications. For example, fabricated Au/CFO nanocomposite with the intrinsic cytotoxic effect on cancer cells can be used as a multifunctial agent in the photothermal therapy and magnetic hyperthermia theranostics of leukemia.

Supplementary Materials: The following are available online at https://www.mdpi.com/article/10.3390/pr9122264/s1, Figure S1: EDX spectrum for CFO nanoparticles; Figure S2: EDX spectrum for Au/CFO nanocomposites; Figure S3: Relative viability of Jurkat cells after 2, 4, 8, 24, and 48 h of exposure with CFO magnetic nanoparticles covered with DHCA and Au/CFO nanocomposite.

Author Contributions: Conceptualization, A.M., S.J. and V.K.B.; Data curation, V.K.B., L.P., V.R. and K.L.; Formal analysis, A.M., V.K.B., D.M., L.G. and K.L.; Funding acquisition, M.S., L.P. and M.V.; Investigation, A.M., S.J., V.K.B., S.P., V.G.K. and A.S.O.; Methodology, A.M., S.J., V.K.B., S.P., V.G.K., A.S.O. and L.G.; Project administration, S.J., V.K.B., V.R. and K.L.; Resources, M.S., V.R., M.V. and K.L.; Software, L.P.; Supervision, S.J., M.S., L.P., V.R., M.V. and K.L.; Validation, S.J., V.R., M.V. and K.L.; Visualization, A.M., V.K.B., L.P. and K.L.; Writing—original draft, A.M., V.K.B., D.M., A.S.O., L.P., M.V. and K.L.; Writing—review & editing, S.J., V.K.B., D.M., L.P., V.R. and K.L. All authors have read and agreed to the published version of the manuscript.

Funding: This work was supported by the Russian Science Foundation, grant No. 21-72-20158 (modeling and experimental studies of optical properties; magnetic measurements; X-ray diffraction analysis; biological experiments). This work was supported by the Slovenian Research Agency (ARRS) Grants J2-8169, N2-0150, and P2-0091 (synthesis of nanocomposites; TEM imaging; Zeta-potential study). S.J. thank the 5 top 100 Russian Academic Excellence Project at the Immanuel Kant Baltic Federal University for funding the synthesis of magnetic nuclei of nanoparticles and mobility support.

Institutional Review Board Statement: The study was conducted according to the guidelines of the Declaration of Helsinki, and approved by the Local Ethics Committee of Innovation park, Immanuel Kant Baltic Federal University (protocol code 5 and 16 May 2016).

Informed Consent Statement: Informed consent was obtained from all subjects involved in the study.

Acknowledgments: Authors acknowledge Natalia D. Gazatova and Larisa S. Litvinova (IKBFU, Kaliningrad, Russian Federation) for kindly providing donor's blood for peripheral blood mononuclear cells (PBMC) isolation. This was done in accordance with permission no. 5 from 16 May 2016; the Local Ethics Committee, Innovation park, Immanuel Kant Baltic Federal University. S.J. thanks to the Ministry of Education, Science and Technological Development of the Republic of Serbia research topic "Physics and Chemistry with ion beams". V.R., V.G.K. and D.M. acknowledge the support of the Ministry of Science and Higher Education of the Russian Federation (The Sophia Kovalevskaya North-West Mathematical Research Center project No. 075-02-2021-1748) for calculations sources.

Conflicts of Interest: The authors declare no conflict of interest.

References

1. Pankhurst, Q.A.; Thanh, N.T.K.; Jones, S.K.; Dobson, J. Progress in applications of magnetic nanoparticles in biomedicine. *J. Phys. D Appl. Phys.* **2009**, *42*, 224001. [CrossRef]
2. Pankhurst, Q.; Jones, S.; Dobson, J. Applications of magnetic nanoparticles in biomedicine: The story so far. *J. Phys. D Appl. Phys.* **2016**, *49*, 501002. [CrossRef]
3. Reddy, L.H.; Arias, J.L.; Nicolas, J.; Couvreur, P. Magnetic Nanoparticles: Design and Characterization, Toxicity and Biocompatibility, Pharmaceutical and Biomedical Applications. *Chem. Rev.* **2012**, *112*, 5818–5878. [CrossRef] [PubMed]
4. Kim, M.; Lee, J.; Nam, J. Plasmonic Photothermal Nanoparticles for Biomedical Applications. *Adv. Sci.* **2019**, *6*, 1900471. [CrossRef]

5. Sharifi, I.; Shokrollahi, H.; Amiri, S. Ferrite-based magnetic nanofluids used in hyperthermia applications. *J. Magn. Magn. Mater.* **2012**, *324*, 903–915. [CrossRef]
6. Abudayyak, M.; Altinçekiç Gürkaynak, T.; Özhan, G. In Vitro Evaluation of the Toxicity of Cobalt Ferrite Nanoparticles in Kidney Cell. *Turkish J. Pharm. Sci.* **2017**, *14*, 169–173. [CrossRef] [PubMed]
7. Aşık, E.; Akpınar, Y.; Güray, N.T.; İşcan, M.; Demircigil, G.Ç.; Volkan, M. Cellular uptake, genotoxicity and cytotoxicity of cobalt ferrite magnetic nanoparticles in human breast cells. *Toxicol. Res.* **2016**, *5*, 1649–1662. [CrossRef]
8. Finetti, F.; Terzuoli, E.; Donnini, S.; Uva, M.; Ziche, M.; Morbidelli, L. Monitoring Endothelial and Tissue Responses to Cobalt Ferrite Nanoparticles and Hybrid Hydrogels. *PLoS ONE* **2016**, *11*, e0168727. [CrossRef]
9. Lucht, N.; Friedrich, R.P.; Draack, S.; Alexiou, C.; Viereck, T.; Ludwig, F.; Hankiewicz, B. Biophysical Characterization of (Silica-coated) Cobalt Ferrite Nanoparticles for Hyperthermia Treatment. *Nanomaterials* **2019**, *9*, 1713. [CrossRef]
10. Pašukonienė, V.; Mlynska, A.; Steponkienė, S.; Poderys, V.; Matulionytė, M.; Karabanovas, V.; Statkutė, U.; Purvinienė, R.; Kraśko, J.A.; Jagminas, A.; et al. Accumulation and biological effects of cobalt ferrite nanoparticles in human pancreatic and ovarian cancer cells. *Medicina* **2014**, *50*, 237–244. [CrossRef]
11. Balakrishnan, P.B.; Silvestri, N.; Fernandez-Cabada, T.; Marinaro, F.; Fernandes, S.; Fiorito, S.; Miscuglio, M.; Serantes, D.; Ruta, S.; Livesey, K.; et al. Exploiting Unique Alignment of Cobalt Ferrite Nanoparticles, Mild Hyperthermia, and Controlled Intrinsic Cobalt Toxicity for Cancer Therapy. *Adv. Mater.* **2020**, *32*, 2003712. [CrossRef]
12. Gupta, R.; Sharma, D. Manganese-Doped Magnetic Nanoclusters for Hyperthermia and Photothermal Glioblastoma Therapy. *ACS Appl. Nano Mater.* **2020**, *3*, 2026–2037. [CrossRef]
13. Espinosa, A.; Di Corato, R.; Kolosnjaj-Tabi, J.; Flaud, P.; Pellegrino, T.; Wilhelm, C. Duality of Iron Oxide Nanoparticles in Cancer Therapy: Amplification of Heating Efficiency by Magnetic Hyperthermia and Photothermal Bimodal Treatment. *ACS Nano* **2016**, *10*, 2436–2446. [CrossRef]
14. Saykova, D.; Saikova, S.; Mikhlin, Y.; Panteleeva, M.; Ivantsov, R.; Belova, E. Synthesis and Characterization of Core–Shell Magnetic Nanoparticles $NiFe_2O_4$@Au. *Metals* **2020**, *10*, 1075. [CrossRef]
15. Pita, M.; Abad, J.M.; Vaz-Dominguez, C.; Briones, C.; Mateo-Martí, E.; Martín-Gago, J.A.; del Puerto Morales, M.; Fernández, V.M. Synthesis of cobalt ferrite core/metallic shell nanoparticles for the development of a specific PNA/DNA biosensor. *J. Colloid Interface Sci.* **2008**, *321*, 484–492. [CrossRef]
16. Jagminas, A.; Mažeika, K.; Kondrotas, R.; Kurtinaitienė, M.; Jagminienė, A.; Mikalauskaitė, A. Functionalization of Cobalt Ferrite Nanoparticles by a Vitamin C-Assisted Covering with Gold. *Nanomater. Nanotechnol.* **2014**, *4*, 11. [CrossRef]
17. Saikova, S.; Pavlikov, A.; Trofimova, T.; Mikhlin, Y.; Karpov, D.; Asanova, A.; Grigoriev, Y.; Volochaev, M.; Samoilo, A.; Zharkov, S.; et al. Hybrid Nanoparticles Based on Cobalt Ferrite and Gold: Preparation and Characterization. *Metals* **2021**, *11*, 705. [CrossRef]
18. Mikalauskaitė, A.; Kondrotas, R.; Niaura, G.; Jagminas, A. Gold-Coated Cobalt Ferrite Nanoparticles via Methionine-Induced Reduction. *J. Phys. Chem. C* **2015**, *119*, 17398–17407. [CrossRef]
19. Smith, M.; McKeague, M.; DeRosa, M.C. Synthesis, transfer, and characterization of core-shell gold-coated magnetic nanoparticles. *MethodsX* **2019**, *6*, 333–354. [CrossRef]
20. Rio, I.S.R.; Rodrigues, A.R.O.; Rodrigues, C.P.; Almeida, B.G.; Pires, A.; Pereira, A.M.; Araújo, J.P.; Castanheira, E.M.S.; Coutinho, P.J.G. Development of Novel Magnetoliposomes Containing Nickel Ferrite Nanoparticles Covered with Gold for Applications in Thermotherapy. *Materials* **2020**, *13*, 815. [CrossRef]
21. Zhang, H.; Wang, J.; Zeng, Y.; Wang, G.; Han, S.; Yang, Z.; Li, B.; Wang, X.; Gao, J.; Zheng, L.; et al. Leucine-coated cobalt ferrite nanoparticles: Synthesis, characterization and potential biomedical applications for drug delivery. *Phys. Lett. A* **2020**, *384*, 126600. [CrossRef]
22. Murphy, C.J.; Gole, A.M.; Stone, J.W.; Sisco, P.N.; Alkilany, A.M.; Goldsmith, E.C.; Baxter, S.C. Gold Nanoparticles in Biology: Beyond Toxicity to Cellular Imaging. *Acc. Chem. Res.* **2008**, *41*, 1721–1730. [CrossRef] [PubMed]
23. Ghosh, P.; Han, G.; De, M.; Kim, C.; Rotello, V. Gold nanoparticles in delivery applications. *Adv. Drug Deliv. Rev.* **2008**, *60*, 1307–1315. [CrossRef] [PubMed]
24. Abadeer, N.S.; Murphy, C.J. Recent Progress in Cancer Thermal Therapy Using Gold Nanoparticles. *J. Phys. Chem. C* **2016**, *120*, 4691–4716. [CrossRef]
25. Daniel, M.C.; Astruc, D. Gold Nanoparticles: Assembly, Supramolecular Chemistry, Quantum-Size-Related Properties, and Applications Toward Biology, Catalysis, and Nanotechnology. *Chem. Rev.* **2004**, *104*, 293–346. [CrossRef]
26. Dreaden, E.C.; Alkilany, A.M.; Huang, X.; Murphy, C.J.; El-Sayed, M.A. The golden age: Gold nanoparticles for biomedicine. *Chem. Soc. Rev.* **2012**, *41*, 2740–2779. [CrossRef]
27. Sztandera, K.; Gorzkiewicz, M.; Klajnert-Maculewicz, B. Gold Nanoparticles in Cancer Treatment. *Mol. Pharm.* **2019**, *16*, 1–23. [CrossRef]
28. Jain, S.; Hirst, D.G.; O'Sullivan, J.M. Gold nanoparticles as novel agents for cancer therapy. *Br. J. Radiol.* **2012**, *85*, 101–113. [CrossRef]
29. Weissleder, R. A clearer vision for in vivo imaging. *Nat. Biotechnol.* **2001**, *19*, 316–317. [CrossRef]
30. Maier, S.A. *Plasmonics: Fundamentals and Applications*; Springer: New York, NY, USA, 2007; ISBN 978-0-387-33150-8.
31. Zhang, Y.; Zhao, Y.; Yang, Y.; Shen, J.; Yang, H.; Zhou, Z.; Yang, S. A bifunctional sensor based on Au-Fe3O4 nanoparticle for the detection of Cd2+. *Sens. Actuators B Chem.* **2015**, *220*, 622–626. [CrossRef]

32. Omelyanchik, A.; Efremova, M.; Myslitskaya, N.; Zybin, A.; Carey, B.J.; Sickel, J.; Kohl, H.; Bratschitsch, R.; Abakumov, M.; Majouga, A.; et al. Magnetic and Optical Properties of Gold-Coated Iron Oxide Nanoparticles. *J. Nanosci. Nanotechnol.* **2019**, *19*, 4987–4993. [CrossRef]
33. Wei, Y.; Klajn, R.; Pinchuk, A.O.; Grzybowski, B.A. Synthesis, Shape Control, and Optical Properties of Hybrid Au/Fe_3O_4 "Nanoflowers". *Small* **2008**, *4*, 1635–1639. [CrossRef]
34. Schick, I.; Gehrig, D.; Montigny, M.; Balke, B.; Panthöfer, M.; Henkel, A.; Laquai, F.; Tremel, W. Effect of Charge Transfer in Magnetic-Plasmonic Au@MO x (M = Mn, Fe) Heterodimers on the Kinetics of Nanocrystal Formation. *Chem. Mater.* **2015**, *27*, 4877–4884. [CrossRef]
35. Umut, E.; Pineider, F.; Arosio, P.; Sangregorio, C.; Corti, M.; Tabak, F.; Lascialfari, A.; Ghigna, P. Magnetic, optical and relaxometric properties of organically coated gold–magnetite (Au–Fe3O4) hybrid nanoparticles for potential use in biomedical applications. *J. Magn. Magn. Mater.* **2012**, *324*, 2373–2379. [CrossRef]
36. Zeng, H.; Sun, S. Syntheses, Properties, and Potential Applications of Multicomponent Magnetic Nanoparticles. *Adv. Funct. Mater.* **2008**, *18*, 391–400. [CrossRef]
37. Gabbani, A.; Fantechi, E.; Petrucci, G.; Campo, G.; de Julián Fernández, C.; Ghigna, P.; Sorace, L.; Bonanni, V.; Gurioli, M.; Sangregorio, C.; et al. Dielectric Effects in FeO x -Coated Au Nanoparticles Boost the Magnetoplasmonic Response: Implications for Active Plasmonic Devices. *ACS Appl. Nano Mater.* **2021**, *4*, 1057–1066. [CrossRef]
38. Yao, C.; Zhang, L.; Wang, J.; He, Y.; Xin, J.; Wang, S.; Xu, H.; Zhang, Z. Gold Nanoparticle Mediated Phototherapy for Cancer. *J. Nanomater.* **2016**, *2016*, 1–29. [CrossRef]
39. Fayazzadeh, S.; Khodaei, M.; Arani, M.; Mahdavi, S.R.; Nizamov, T.; Majouga, A. Magnetic Properties and Magnetic Hyperthermia of Cobalt Ferrite Nanoparticles Synthesized by Hydrothermal Method. *J. Supercond. Nov. Magn.* **2020**, *33*, 2227–2233. [CrossRef]
40. Verde, E.L.; Landi, G.T.; Gomes, J.A.; Sousa, M.H.; Bakuzis, A.F. Magnetic hyperthermia investigation of cobalt ferrite nanoparticles: Comparison between experiment, linear response theory, and dynamic hysteresis simulations. *J. Appl. Phys.* **2012**, *111*, 123902. [CrossRef]
41. Blanco-Andujar, C.; Walter, A.; Cotin, G.; Bordeianu, C.; Mertz, D.; Felder-Flesch, D.; Begin-Colin, S. Design of iron oxide-based nanoparticles for MRI and magnetic hyperthermia. *Nanomedicine* **2016**, *11*, 1889–1910. [CrossRef]
42. Kayal, S.; Ramanujan, R.V. Anti-Cancer Drug Loaded Iron–Gold Core–Shell Nanoparticles (Fe@Au) for Magnetic Drug Targeting. *J. Nanosci. Nanotechnol.* **2010**, *10*, 5527–5539. [CrossRef]
43. Şologan, M.; Padelli, F.; Giachetti, I.; Aquino, D.; Boccalon, M.; Adami, G.; Pengo, P.; Pasquato, L. Functionalized Gold Nanoparticles as Contrast Agents for Proton and Dual Proton/Fluorine MRI. *Nanomaterials* **2019**, *9*, 879. [CrossRef]
44. Jovanović, S.; Spreitzer, M.; Tramšek, M.; Trontelj, Z.; Suvorov, D. Effect of Oleic Acid Concentration on the Physicochemical Properties of Cobalt Ferrite Nanoparticles. *J. Phys. Chem. C* **2014**, *118*, 13844–13856. [CrossRef]
45. Kostevšek, N.; Hudoklin, S.; Kreft, M.E.; Serša, I.; Sepe, A.; Jagličić, Z.; Vidmar, J.; Ščančar, J.; Šturm, S.; Kobe, S.; et al. Magnetic interactions and in vitro study of biocompatible hydrocaffeic acid-stabilized Fe–Pt clusters as MRI contrast agents. *RSC Adv.* **2018**, *8*, 14694–14704. [CrossRef]
46. Vukomanović, M.; Logar, M.; Škapin, S.D.; Suvorov, D. Hydroxyapatite/gold/arginine: Designing the structure to create antibacterial activity. *J. Mater. Chem. B* **2014**, *2*, 1557–1564. [CrossRef]
47. Bohren, C.F.; Huffman, D.R. *Absorption and Scattering of Light by Small Particles*; Wiley: Hoboken, NJ, USA, 1998; ISBN 9780471293408.
48. Muscas, G.; Jovanović, S.; Vukomanović, M.; Spreitzer, M.; Peddis, D. Zn-doped cobalt ferrite: Tuning the interactions by chemical composition. *J. Alloys Compd.* **2019**, *796*, 203–209. [CrossRef]
49. Ng, E.Y.K.; Kumar, S.D. Physical mechanism and modeling of heat generation and transfer in magnetic fluid hyperthermia through Néelian and Brownian relaxation: A review. *Biomed. Eng. Online* **2017**, *16*, 36.
50. Carrey, J.; Mehdaoui, B.; Respaud, M. Simple models for dynamic hysteresis loop calculations of magnetic single-domain nanoparticles: Application to magnetic hyperthermia optimization. *J. Appl. Phys.* **2011**, *109*, 083921. [CrossRef]
51. Kush, P.; Kumar, P.; Singh, R.; Kaushik, A. Aspects of high-performance and bio-acceptable magnetic nanoparticles for biomedical application. *Asian J. Pharm. Sci.* **2021**. [CrossRef]
52. Yeshchenko, O.A.; Kutsevol, N.V.; Naumenko, A.P. Light-Induced Heating of Gold Nanoparticles in Colloidal Solution: Dependence on Detuning from Surface Plasmon Resonance. *Plasmonics* **2016**, *11*, 345–350. [CrossRef]
53. Palik, E.D. *Handbook of Optical Constants of Solids*; Academic Press: Cambridge, MA, USA, 1998; Volume 3.
54. Pinchuk, A.; Kreibig, U. Interface decay channel of particle surface plasmon resonance. *New J. Phys.* **2003**, *5*, 151. [CrossRef]
55. Horev-Azaria, L.; Baldi, G.; Beno, D.; Bonacchi, D.; Golla-Schindler, U.; Kirkpatrick, J.C.; Kolle, S.; Landsiedel, R.; Maimon, O.; Marche, P.N.; et al. Predictive Toxicology of cobalt ferrite nanoparticles: Comparative in-vitro study of different cellular models using methods of knowledge discovery from data. *Part. Fibre Toxicol.* **2013**, *10*, 32. [CrossRef] [PubMed]
56. Ahmad, F.; Zhou, Y. Pitfalls and Challenges in Nanotoxicology: A Case of Cobalt Ferrite ($CoFe_2O_4$) Nanocomposites. *Chem. Res. Toxicol.* **2017**, *30*, 492–507. [CrossRef] [PubMed]
57. Mmelesi, O.K.; Masunga, N.; Kuvarega, A.; Nkambule, T.T.; Mamba, B.B.; Kefeni, K.K. Cobalt ferrite nanoparticles and nanocomposites: Photocatalytic, antimicrobial activity and toxicity in water treatment. *Mater. Sci. Semicond. Process.* **2021**, *123*, 105523. [CrossRef]

58. Nam, P.H.; Phuc, N.X.; Manh, D.H.; Tung, D.K.; Nguyen, V.Q.; Nam, N.H.; Son, P.K.; Bach, T.N.; Phong, P.T. Physical characterization and heating efficacy of chitosan-coated cobalt ferrite nanoparticles for hyperthermia application. *Phys. E Low-Dimens. Syst. Nanostructures* **2021**, *134*, 114862. [CrossRef]
59. Wang, G.; Zhou, F.; Li, X.; Li, J.; Ma, Y.; Mu, J.; Zhang, Z.; Che, H.; Zhang, X. Controlled synthesis of L-cysteine coated cobalt ferrite nanoparticles for drug delivery. *Ceram. Int.* **2018**, *44*, 13588–13594. [CrossRef]
60. Hatamie, S.; Parseh, B.; Ahadian, M.M.; Naghdabadi, F.; Saber, R.; Soleimani, M. Heat transfer of PEGylated cobalt ferrite nanofluids for magnetic fluid hyperthermia therapy: In vitro cellular study. *J. Magn. Magn. Mater.* **2018**, *462*, 185–194. [CrossRef]
61. Wang, H.-H.; Su, C.-H.; Wu, Y.-J.; Lin, C.-A.J.; Lee, C.-H.; Shen, J.-L.; Chan, W.-H.; Chang, W.H.; Yeh, H.-I. Application of Gold in Biomedicine: Past, Present and Future. *Int. J. Gerontol.* **2012**, *6*, 1–4. [CrossRef]
62. Singh, P.; Pandit, S.; Mokkapati, V.R.S.S.; Garg, A.; Ravikumar, V.; Mijakovic, I. Gold Nanoparticles in Diagnostics and Therapeutics for Human Cancer. *Int. J. Mol. Sci.* **2018**, *19*, 1979. [CrossRef]
63. Jones, C.F.; Grainger, D.W. In vitro assessments of nanomaterial toxicity. *Adv. Drug Deliv. Rev.* **2009**, *61*, 438–456. [CrossRef]